Available online at www.sciencedirect.com
SCIENCE DIRECT®
BioSystems 79 (2005) 213–222
BioSystems
www.elsevier.com/locate/biosystems

A new method for adjusting neural response jitter in the STRF obtained by spike-trigger averaging

Tsai-Rong Chang[a], Pau-Choo Chung[a], Tzai-Wen Chiu[b], Paul Wai-Fung Poon[c,*]

[a] *Department of Electrical Engineering, National Cheng Kung University, Tainan, Taiwan*
[b] *Institute of Basic Medical Sciences, National Cheng Kung University, Tainan, Taiwan*
[c] *Department of Physiology, College of Medicine, National Cheng Kung University, Tainan, Taiwan*

Abstract

Sensitivity of central auditory neurons to frequency modulated (FM) sound is often characterized based on spectro-temporal receptive field (STRF), which is generated by spike-trigger averaging a random stimulus. Due to the inherent property of time variability in neural response, this method erroneously represents the response jitter as stimulus jitter in the STRF. To reveal the trigger features more clearly, we have implemented a method that minimizes this error. Neural spikes from the brainstem of urethane-anesthetized rats were first recorded in response to two sets of FM stimuli: (a) a random FM tone for the generation of STRF and (b) a family of linear FM ramps for the determination of FM 'trigger point'. Based on the first dataset, STRFs were generated using spike-trigger averaging. Individual modulating waveforms were then matched with respect to their mean waveform at time-windows of a systematically varied length. A stable or optimal variance time profile was found at a particular window length. At this optimal window length, we performed delay adjustments. A marked sharpening in the FM bands in the STRF was found. Results were consistent with the FM 'trigger point' as estimated by the linear FM ramps. We concluded that the present approach of adjusting response jitter was effective in delineating FM trigger features in the STRF.

Keywords: FM sensitivity; Spectro-temporal receptive field; Trigger point; Midbrain auditory neurons; Inferior colliculus

1. Introduction

The knowledge on what features in the complex stimuli are effective to evoke responses of auditory neurons is important for understanding neural mechanisms underlying speech sound coding. In the mammalian vocalization sounds, there are spectral patterns containing time-varying components or features like frequency modulation (FM) or amplitude modulation (AM) (Saberi and Hafter, 1995). Along the ascending auditory pathways, many FM-sensitive neurons appear in substantial proportions, first at the auditory midbrain and subsequently at the auditory cortex (Whitfield and Evans, 1965; Clopton and Win-

* Corresponding author. Tel.: +886 6 235 3535x5458; fax: +886 6 236 2780.
E-mail address: ppoon@mail.ncku.edu.tw (P.W.-F. Poon).

0303-2647/$ – see front matter © 2004 Elsevier Ireland Ltd. All rights reserved.
doi:10.1016/j.biosystems.2004.09.027

field, 1974; Rees and Moller, 1983; Philips et al., 1985; Poon et al., 1991, 1992; Chiu et al., 1998; DeCharms et al., 1998; Heil and Irvine, 1998; Keller and Takahashi, 2000; Chiu and Poon, 2000; Poon and Yu, 2000; Poon and Chiu, 2000; Escabi and Schreiner, 2002; Linden et al., 2003). To understand the mechanisms of speech sound coding, detailed knowledge on the triggering features of FM-sensitive neurons is of obvious importance.

FM sensitivity of an auditory neuron is frequently characterized based on its spectro-temporal receptive field (STRF) (Eggermont et al., 1983; DeCharms et al., 1998; Poon and Yu, 2000; Depireux et al., 2001; Rutkowski et al., 2002; Escabi and Schreiner, 2002). Typically, a STRF is generated using spike-trigger averaging of a random stimulus. There are several approaches that differ mainly in the stimulus they employed. The following stimuli have been used: viz. (a) white noise (Kim and Young, 1994); (b) random chord noise (DeCharms et al., 1998); (c) dynamic ripple noise (Klein et al., 2000; Depireux et al., 2001; Escabi and Schreiner, 2002); and (d) random FM tone (Poon et al., 1992; Kao et al., 1997; Poon and Yu, 2000). While each approach may have its own strength and weakness, they all suffer from one major drawback, i.e., the trigger features revealed in the STRFs are often blur in appearance or hard to delineate fine structures (e.g., DeCharms et al., 1998; Poon and Yu, 2000). That is mainly because an important aspect of the response has been over-looked, viz. the response jitter. Response jitter, or specifically the variation in response latency across identical stimulus trials, is widely observed in responses of central neurons to a number of sensory stimuli (Hubel and Wiesel, 1959; Buracas et al., 1998; Lee et al., 1998; Shadlen and Newsome, 1998; Mazurek and Shadlen, 2002; DeWeese et al., 2003). It is generally considered to reflect the inherent properties of synaptic circuitry (Marsalek et al., 1997) or simply synaptic noise (Shadlen and Newsome, 1998). Since spike-trigger averaging would need to align the time of occurrence of neural spikes, STRF always erroneously represents response jitter as stimulus jitter. Consequently, the trigger features in the STRF would appear blurred. To reveal the trigger features more clearly, we implemented in the present study a novel method to minimize this error and we were able to show significant improvements on STRFs of a number of midbrain auditory neurons in the rat.

2. Materials and methods

Rats (Sprague–Dawley, body weight 200–250 g) were anesthetized with urethane (1.5 g/kg, i.p.), and mounted on a special head holder. The animal was placed inside a sound-treated chamber (Industrial Acoustic Corporation) to allow free-field acoustic stimulation and extra-cellular single unit recordings using conventional electrophysiological procedures. The skull overlying the occipital cortex was surgically opened and glass micropipette electrode (impedance 20–70 MΩ) was advanced into the midbrain inferior colliculus (IC) with a stepping micro-drive (Narishige) to detect single units that responded to an intensive click (0.1 ms pulse, >90 dB SPL). After an auditory unit had been identified, its responses to a series of acoustic signals were recorded with a computer interface (Tucker Davies Technology System II) after proper amplification and filtering (Axonprobe 1A, PARC-5113).

Two sets of FM stimuli were adopted. The first one was a random FM tone. It was generated by low-pass filtering a white noise digitally (at either 12.5, 25 or 125 Hz), and then the signal was connected to the voltage-control frequency input of a function generator (Tektronix FG280) to control the instantaneous frequency of a continuous sine wave. The result was an FM tone, the frequency of which was varied basically in a random manner. Such FM stimuli have been shown to be powerful in activating auditory neurons in the rat IC (Poon et al., 1991). After determining the most sensitive frequency or characteristic frequency (CF) of the unit, the carrier frequency of the random FM tone was set at the CF with a modulating range about two to three octave wide. For each unit, spike responses were collected at the three different FM tones. For every neuron, only the dataset with the largest amount of spikes was used for subsequent analysis. Each dataset was the result of 2 min of continuous stimulation.

The second FM stimulus was a family of linear FM ramps. Similar to the random FM tones, the modulating waveform was first generated digitally to control the instantaneous frequency of the sine wave generator. It consisted of a series of systematically varied triangular linear FM ramps ($n = 6$) delivered intermittently over a period of 2 s (see Fig. 5a). The series of FM ramps had up- and down-sweep phases with modulation rates basically overlapping with those of the random FM tones (FM rates from 9.8 to 63.2 octave/s, range 1.58 octave).

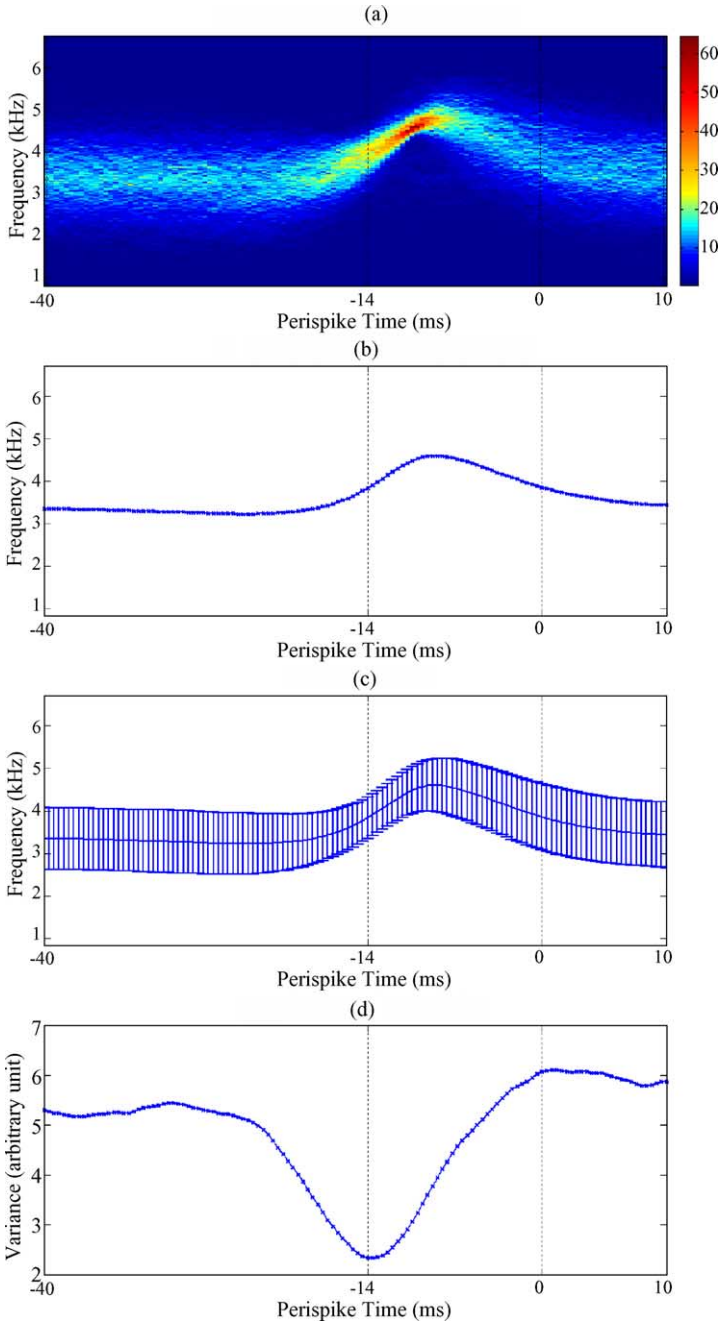

Fig. 1. STRF-related statistics of a representative FM-sensitive neuron in the IC. (a) STRF in color-coded pixel map where the color of each pixel represents the number of overlapping peri-spike modulating time waveforms (see color scale) ($n = 1863$ tracings). A maximum concentration (red pixels) appears halfway along the rising slope. (b) Mean frequency time profile (MFTP) of peri-spike modulating time waveforms. (c) MFTP is shown together with standard deviation (S.D.) at each time point. (d) The corresponding variance time profile (VTP) showing a minimum (vertical line at −11 ms) that precedes the most concentrated region shown in the STRF of the top panel.

During experiment, a computer interface (Tucker Davies Technology System II) was programmed to deliver the modulating waveforms and it simultaneously collected spike responses (after being conditioned into 0.4 ms, 5 V rectangular pulses) at a sampling interval of 0.4 ms. Details of electrophysiological procedures for extra-cellular recording could be found in the previous publications from this laboratory (Poon et al., 1991; Chiu and Poon, 2000).

2.1. Generation of STRF and its statistics

In a typical response dataset of 2 min collected from an FM-sensitive neuron, there were over 1000 of spike responses. A 50 ms time-window was applied to extract short segments of the peri-spike modulating waveforms. The extracted modulating waveforms (40 ms pre-spike, 10 ms post-spike) were overlaid in a frequency–versus–time plot and displayed as STRF or a color-coded pixel map representing the place and extent of overlaps in the pre-spike stimulus. The parts with concentrated overlaps represented the trigger features (Poon and Yu, 2000). Fig. 1a shows such a representative STRF of an IC unit that responds selectively to FM stimulation. The highly overlapped area often appeared in the form of an elongated structure representing an FM band. The spectral extent and slope of this FM band reflected the preferred stimulus features of the cell (e.g., the preferred range and preferred rate of modulation). The FM trigger features could also be visualized simply by averaging the peri-spike modulating waveforms (Fig. 1b) to result in a mean fre-

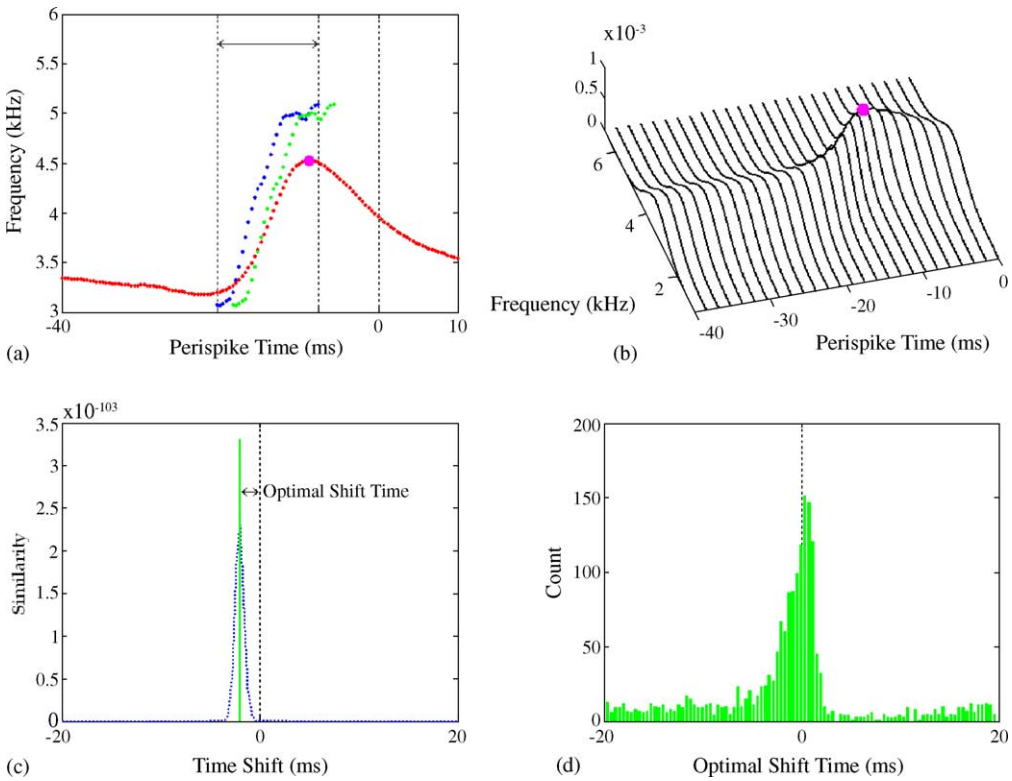

Fig. 2. Method of determining the optimal shift time (OST) for individual modulating waveforms. (a) An individual modulating waveform (blue dotted-line) and one of its time-shifted versions (green dotted-line) are displayed within a selected window length (arrows) to match with the MFTP (red dotted-line). (b) Estimated normal distributions of the modulating waveforms around the mean value at each point of the MFTP are displayed in perspective plot (the peak of MFTP is marked by a red dot, same position as in (a)). (c) The Similarity Index (SI) function between the time-shifted modulating waveform (within a range of +/−20 ms) and the MFTP shows a peak value corresponded to the optimal shift time (arrows). (d) The distribution of OST for all the modulating waveforms ($n = 1863$) is shown in histogram.

quency time profile (MFTP). The standard deviation or variance at each point of the MFTP was plotted to produce a variance time profile (VTP) (Fig. 1c–d) to reflect the packing density of waveform tracings in the STRF. Invariably a minimum could be found in VTP that was located within the time span of the FM band.

2.2. Determination of optimal shift time (OST)

We first determined the time point where the VTP displayed a minimum (Fig. 1d). Then we created a short-time window of a preset length (from about 5 to 15 ms at steps of 1–2 ms) centered at this time point. The portions of the modulating time waveforms fell within this time-window were then extracted. Each of the extracted waveforms was shifted systematically along the time axis over a range of ±20 ms, at steps of 0.4 ms (Fig. 2a). At each step of shift time, the similarity between the shifted modulating time waveform and the original MFTP was estimated (Fig. 2b) using a 'similarity index' (SI) as defined by the following equation:

$$p_i = \frac{1}{\sqrt{2\pi\sigma_i^2}} e^{-(f_i-\eta_i)^2/2\sigma_i^2} \qquad \text{Similarity} = \prod_{i=1}^{\max t} p_i$$

A number of SI were produced according to different shift times (Fig. 2c). We then determined the shift time at the maximum SI, or the 'optimal shift time' (OST) for this modulating time waveform (Fig. 2c). This procedure of OST determination was

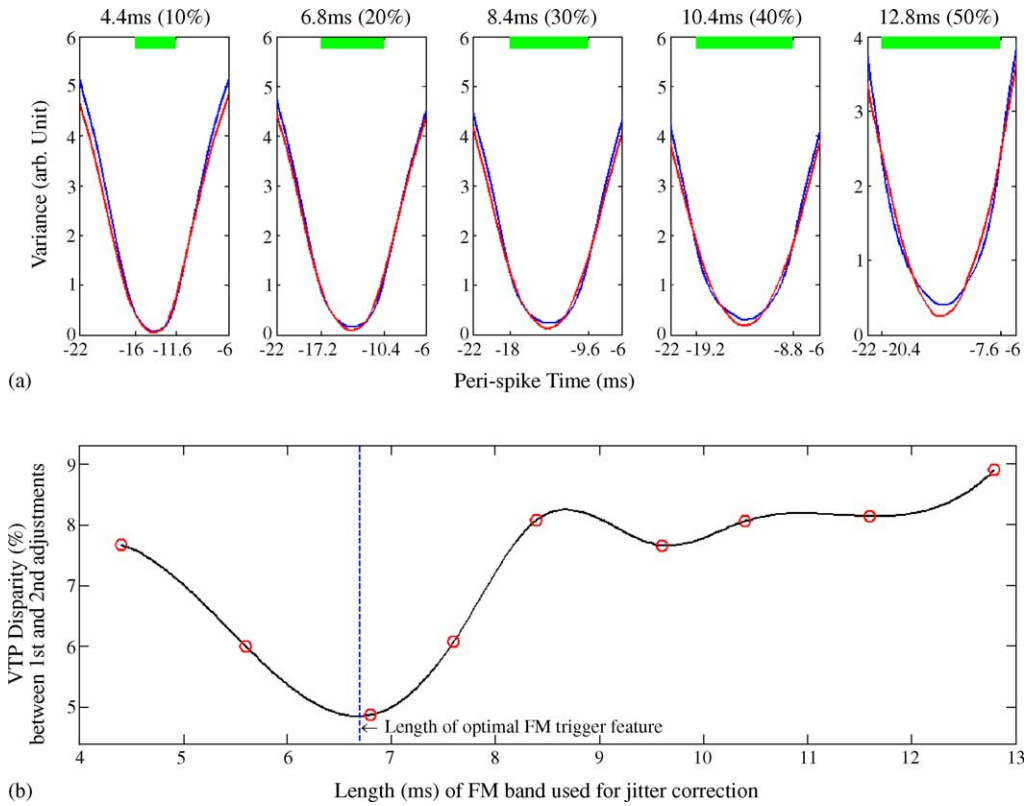

Fig. 3. (a) Variance time profiles (VTP) after the first-time and second-time jitter adjustments (blue and red tracings, respectively) are shown at five systematically varied time-windows. The corresponding length of time-window is marked by the green bars. (b) Disparity between the VTP after first- and second-time jitter adjustments is represented by the disparity index and plotted as a function of time-window length (spline curve-fitting). A minimum in the disparity function (vertical dash line) is taken to represent an optimal time-window (OTW). This OTW is used for jitter adjustment to produce a new STRF as shown in Fig. 4.

applied for all of the modulating waveforms constituting the STRF, and the distribution of the corresponding OSTs was shown in a histogram (Fig. 2d). Subsequently, we shifted all modulating time waveforms according to their respective OSTs. A first-time adjusted MFTP was generated together with its new VTP. This procedure of OST determination was again repeated for the second-time using the same time-window. The only difference was that the SI was calculated against the adjusted MFTP instead of its original version. Subsequently a second-time adjusted MFTP was produced together with its new VTP.

2.3. Determination of the optimal time-window (OTW)

After obtaining the first- and second-time adjusted VTPs at a given time-window, we then assessed the disparity between the two VTPs using a 'disparity index' (DI) (Fig. 3a) as defined by the following equation:

$$\text{Disparity} = \frac{\sum_{i=\text{left}}^{\text{right}} \max(f_{1\text{st},i}, f_{2\text{nd},i}) - \sum_{i=\text{left}}^{\text{right}} \min(f_{1\text{st},i}, f_{2\text{nd},i})}{\sum_{i=\text{left}}^{\text{right}} \max(f_{1\text{st},i}, f_{2\text{nd},i})}$$

A family of DI generated at different time-windows (Fig. 3b) was used to determine the specific time-window when the shift time adjustment had reached a stable level. Our working hypothesis was that, if the time-window had been chosen to overlap exactly with the extent of the FM trigger features, there should be minimal disparity between the first and second VTPs. Otherwise, the adjustment time-window may have set either too long to include irrelevant portions of the modulating waveforms, or set too short to exclude relevant

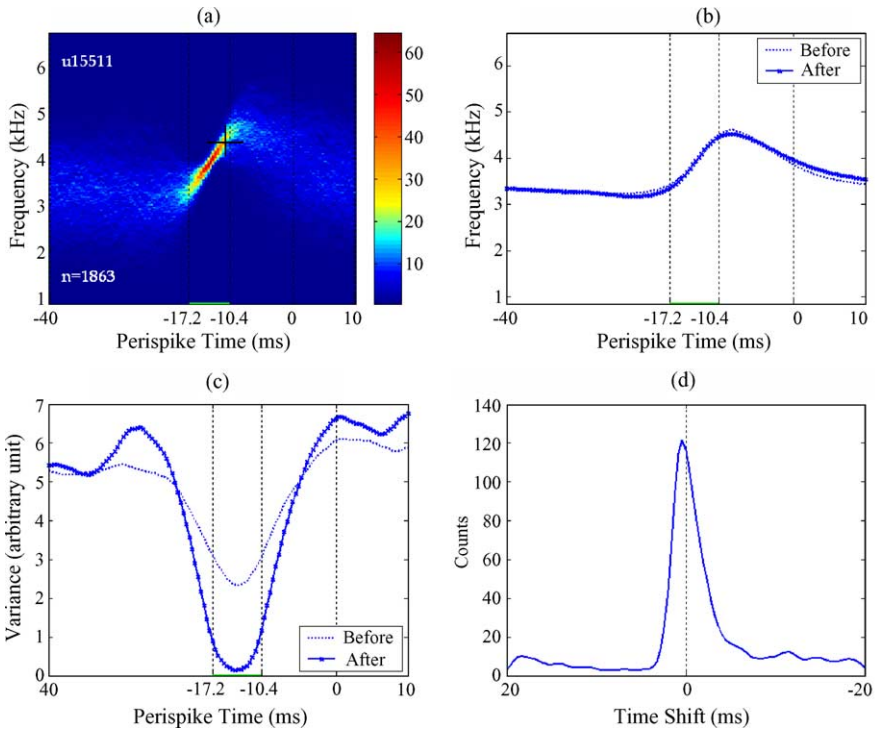

Fig. 4. STRF after jitter adjustment (a) and its related statistics. For comparison, the original MFTP and VTP are also shown in (b), and (c) (thin lines). (d) Distribution of optimal shift times shown in a smoothed histogram. Note a mirror image relationship with the histogram profile as shown in Fig. 2d. Black cross in (a) marks the position of the 'trigger point' (see also Figs. 5 and 6).

portions of the modulating waveforms. In either case, the VTP will continue to vary on repeated procedures of adjustment. In fact, the series of DI thus obtained showed a minimum value corresponded to an 'optimal time-window' (OTW) (Fig. 3b). We adopted this OTW to generate a new STRF using the corresponding OST for each peri-spike modulating waveform (Fig. 4).

2.4. Determination of 'trigger point'

Based on the responses to the second set of FM stimuli (linear FM ramps of different slopes or periods), we further estimated the 'trigger point' of the neuron to FM stimulation. For each FM ramp (Fig. 5a), we constructed the peri-stimulus time histogram (PSTH) based on the spike responses (Fig. 5b–c). The size of the peak in the PSTH represented the probability of neural response to the stimulus. The width of the PSTH peak represented the extent of response jitter. The central transmission delay represented the time lapse between the onset of stimulus to the time when the spike response occurred. Presumably, the effective FM sweep must have gone through the FM feature the cell preferred. This stimulus feature has been called the 'trigger point' in an earlier study (Poon and Yu, 2000). Hence, a family of PSTH was obtained at different FM ramps, and a plot of delay times (y) against the periods of FM ramp (x) displayed a linear relationship that can be approximated by a straight line: $y = ax + b$ through linear regression. The slope (a) and intercept (b) repre-

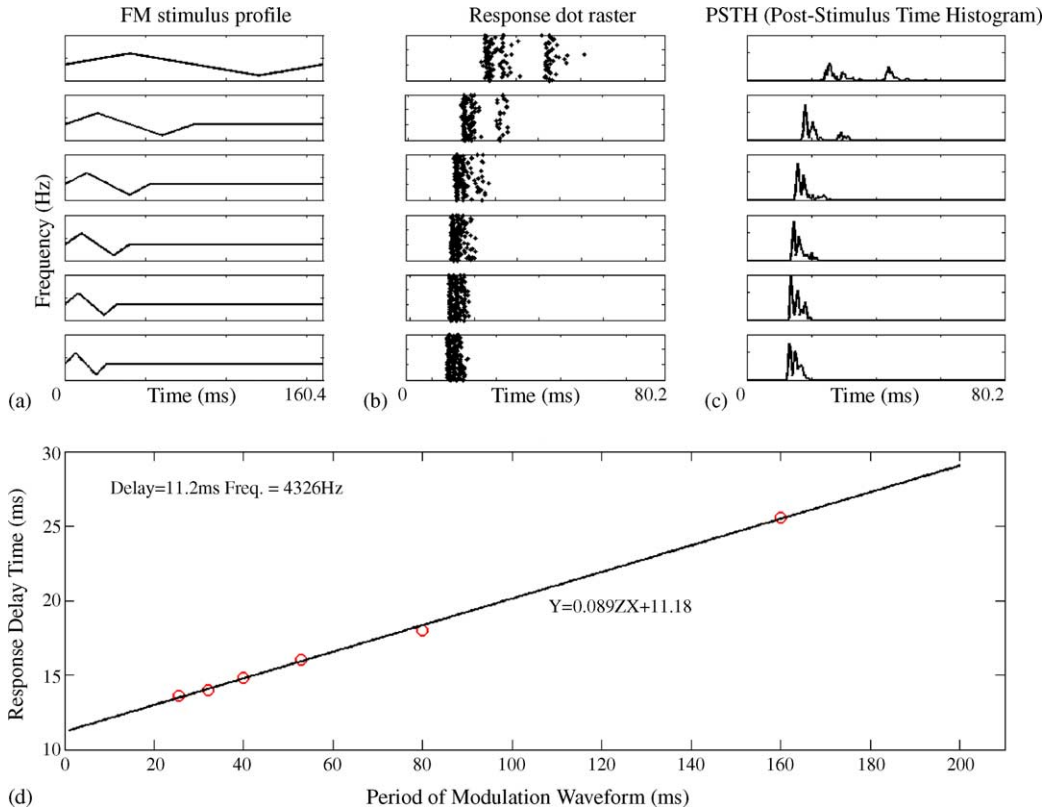

Fig. 5. Determination of the 'trigger point' based on response latencies to systematically varied FM ramps (same neuron as in Figs. 1–4). (a) Instantaneous frequency profiles of the FM stimulus of systematically varied slopes. (b) The corresponding spike responses shown in dot raster (to 60 repeated stimulus trials). Each dot represents a single action potential recorded from the same cell. (c) The corresponding peri-stimulus time histograms (PSTHs). (d) PSTH peak latency (with respect to the start of the corresponding FM ramp) is plotted as a function of the period of the FM stimulus. Data points are fitted with a linear function ($y = ax + b$). The y-intercept represents the 'central transmission time' of the stimulus from the source to the neuron. The slope represents the phase or frequency point on the FM ramp at which the cell is activated after the central transmission time. The same 'trigger point' is also marked in the jitter-adjusted STRF (see Fig. 4a).

sented the phase and central transmission delay time, respectively. From the phase, we could easily calculate the frequency point on the linear ramp. This frequency point represents the ending-frequency or frequency of the 'trigger point' (Poon and Yu, 2000).

3. Results

STRFs, after jitter adjustment, showed marked changes in detailed features even though the gross appearance remained similar. Specifically, the somewhat blurred FM band that presumably reflected the FM trigger features now appears more sharply demarcated. In the new STRF, we could almost always found a short straight FM band (e.g., Fig. 4a). With such unprecedented degree of clarity in the STRF, both the starting- and ending frequencies and the slope of the FM sweep could be readily determined and can be compared with the 'trigger point' results estimated from the second FM stimulus.

Two parameters of the FM band were first extracted from the adjusted STRF: (a) sweep speed or FM slope and (b) the ending-frequency or end-point of the FM band. From the second dataset collected from the same cell using linear FM ramps, a preferred FM ramp associated with the largest amount of spike response was determined. We found that the slope of the FM band

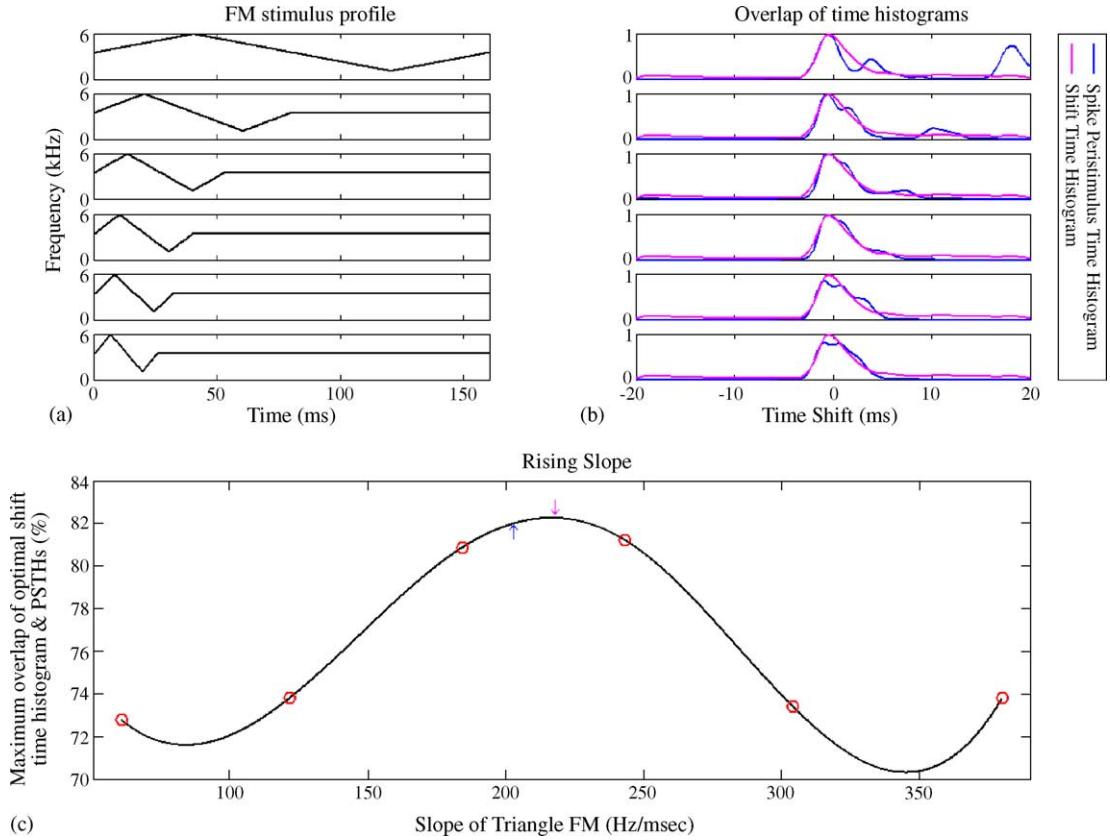

Fig. 6. Frequency time profiles of the FM ramps (a) and (b) the corresponding spike responses to 60 repeated stimuli shown in PSTH (pink tracings) (same data as in Fig. 5. The OST histograms (blue tracings) are shown after systematically optimizing both the shift and PSTH peak value (see also Fig. 4d. To facilitate comparison, tracings in (b) are smoothened by low-pass-filtering of the original histograms. (c) The similarity between the OPT histogram and the PSTH is expressed as the degree of overlap regarding area under the curve, and plotted against the slope of the corresponding FM ramps. Maximal similarity is represented by the peak (pink arrow) after curve fitting data points with a spline function. For comparison, the FM slope from the jitter-adjusted STRF (Fig. 4a is also shown (blue arrow).

in the adjusted STRF, fell close to the preferred linear FM ramp (Fig. 4). Results of estimating 'trigger point' (cross in Fig. 4a) also show remarkable proximity to end-point of the FM band.

Finally, we also examined the similarity in the PSTH of the best FM linear ramp with the histogram of OST. We found that the profile of corresponding PSTH also gave the best fit in terms of maximum overlap with the OST histogram (Fig. 6).

Results similar to those shown above were observed in 10 of 12 IC units we have examined. In the two exceptional units, there was the presence of double spikes at short time intervals.

4. Discussion

The present method of response-time adjustment has been shown to be effective in correcting the stimulus jitter and resulted in an unprecedented clarity of the STRF. Several lines of evidence appeared to support the adequacy of the current method. They include: (a) the matching of 'trigger point' with the FM band in the adjusted STRF; (b) the matching of preferred FM slope in the adjusted STRF with the best FM slope determined by linear FM ramps; and (c) the matching of OST histogram with the profile of PSTH at the corresponding best FM ramp.

In our method of shift time adjustment, we have assumed a basically Gaussian distribution of spike response times. In fact, a test for similarity with Gaussian was positive for all PSTH profiles in the dataset of FM ramps. It was somewhat surprising to find that even the skewness in the OST histogram also matched well with the empirical PSTH (Fig. 6b).

The proximity of 'trigger point' to the end-point of preferred FM band in the adjusted STRF seemed to fit our working hypothesis, which was: (a) if the STRF indeed represented the trigger FM feature, then a linear FM ramp of the same sweep speed should evoke maximal response from the cell; (b) the end-point of the FM band should be a 'trigger point' which represents the ending frequency of the effective FM band. From the 'trigger point' to the activation of the neural spike, there should be a central transmission delay. The central transmission delay time of the 12 neurons was also quite consistent with the known response delay times of IC neurons in the rat.

The small proportion of neurons (2 out of the 12) that failed to produce a satisfactory result after jitter adjustment. In particular, the trigger point failed to fall close to the end of the FM band. This discrepancy could well be related to their double spike discharges. Since our method of computing for MFTP would be affected by the presence of double or multiple spike discharges. Whether or not a preprocessing of the multiple spikes into single spikes would produce better results can be confirmed in future experiments. However, from our randomly selected datasets in the auditory system, single spike responses are probably prevalent enough to allow our method to work for many FM cells.

Acknowledgment

Supported by Academic Excellence Program (89-B-FA08-1-4), Ministry of Education, Taiwan.

References

Buracas, G.T., Zado, A.M., DeWeese, M.R., Albright, T.D., 1998. Efficient discrimination of temporal patterns by motion-sensitive neurons in primate visual cortex. Neuron 20, 959–969.

Chiu, T.W., Liu, Y.D., Poon, P.W.F., 1998. Transient frequency and intensity sensitivities of central auditory neurons estimated with sweep tone—a new approach. Chin. J. Physiol. 41, 133–138.

Chiu, T.W., Poon, P.W.F., 2000. Similarities of FM and AM receptive space representation of single units at the auditory midbrain. Biosystems 58, 229–237.

Clopton, B.M., Winfield, J.A., 1974. Unit responses in the inferior colliculus of rat to temporal auditory patterns of tone sweeps and noise bursts. Exp. Neurol. 42, 532–540.

DeCharms, R.C., Blacke, D.T., Merzenich, M.M., 1998. Optimizing sound features for cortical neurons. Science 280, 1439–1442.

Depireux, D.A., Simon, J.Z., Klein, D.J., Shamma, S.A., 2001. Spectro-temporal response field characterization with dynamic ripples in ferret primary auditory cortex. J. Neurophysiol. 85, 1220–1234.

DeWeese, M.R., Wehr, M., Zador, A.M., 2003. Binary spiking in auditory cortex. J. Neurosci. 23, 7940–7949.

Eggermont, J.J., Sersten, A.M., Johannesma, P.I., 1983. Prediction of the responses of auditory neurons in the midbrain of grass frog based on the spectro-temporal receptive field. Hear. Res. 10, 191–202.

Escabi, M.A., Schreiner, C.E., 2002. Nonlinear spectrotemporal sound analysis by neurons in the auditory midbrain. J. Neurosci. 22, 4114–4131.

Heil, P., Irvine, D.R.F., 1998. Functional specialization in auditory cortex: responses to frequency-modulated stimuli in the cat's posterior auditory fields. J. Neurophysiol. 79, 3041–3059.

Hubel, D.H., Wiesel, T.N., 1959. Receptive fields of single neurons in the cat's striate cortex. J. Physiol. (London) 148, 574–591.

Kao, M.C., Poon, P.W.F., Sun, X., 1997. Modeling of the response of midbrain auditory neurons in the rat to their vocalization sounds based on FM sensitivities. Biosystems 40, 103–109.

Keller, C.H., Takahashi, T.T., 2000. Representation of temporal features of complex sounds by the discharge patterns of neurons in the owl's inferior colliculus. J. Neurophysiol. 84, 2638–2650.

Kim, P.J., Young, E.D., 1994. Comparative analysis of spectrotemporal receptive fields, reverse correlation functions, and frequency tuning curves of auditory-nerve fibers. J. Acoust. Soc. Am. 95, 410–422.

Klein, D.J., Depireux, D.A., Simon, J.Z., Shamma, S.A., 2000. Robust spectrotemporal reverse correlation for the auditory system: optimizing stimulus design. J. Comput. Neurosci. 9, 85–111.

Lee, D., Port, N.L., Kruse, W., Georgopoulos, A.P., 1998. Variability and correlated noise in the discharge of neurons in motor and parietal areas of the primate cortex. J. Neurosci. 18, 1161–1170.

Linden, J.F., Liu, R.C., Sahani, M., Schreiner, C.E., Merzenich, M.M., 2003. Spectrotemporal structure of receptive fields in areas AI and AAF of mouse auditory cortex. J. Neurophysiol. 90, 2660–2675.

Marsalek, P., Koch, C., Maunsell, J., 1997. On the relationship between synaptic inputs and spike output jitter in individual neurons. Proc. Natl. Acad. Sci. U.S.A. 94, 735–740.

Mazurek, M.E., Shadlen, M.N., 2002. Limits to the temporal fidelity of cortical spike rate signals. Nat. Neurosci. 5, 463–471.

Philips, D.P., Mendelson, J.R., Cynader, M.S., Douglas, R.M., 1985. Responses of single neurons in cat auditory cortex to time-varying stimuli: frequency modulated tones of narrow excursion. Exp. Brain Res. 83, 598–601.

Poon, P.W.F., Chen, X., Hwang, J.C., 1991. Basic determinants for FM responses in the inferior colliculus of rats. Exp. Brain Res. 83, 598–601.

Poon, P.W.F., Chen, X., Cheung, Y.M., 1992. Differences in FM response correlate with morphology of neurons in the rat inferior colliculus. Exp. Brain Res. 91, 94–104.

Poon, P.W.F., Chiu, T.W., 2000. Similarities of FM and AM receptive space of single units at the auditory midbrain. Biosystems 58, 229–237.

Poon, P.W.F., Yu, P.P., 2000. Spectro-temporal receptive fields of midbrain auditory neurons in the rat obtained with frequency modulated stimulation. Neurosci. Lett. 289, 9–12.

Rees, A., Moller, A.R., 1983. Responses of neurons in the inferior colliculus of the rat to AM and FM tones. Hear. Res. 10, 301–330.

Rutkowski, R.G., Shackleton, T.M., Schnupp, J.W., Wallace, M.N., Palmer, A.R., 2002. Spectrotemporal receptive field properties of single units in the primary, dorsocaudal and ventrorostral auditory cortex of the guinea pig. Audiol. Neurootol. 7, 214–227.

Saberi, K., Hafter, E.R., 1995. A common neural code for frequency- and amplitude-modulated sounds. Nature 374, 537–539.

Shadlen, M.N., Newsome, W.T., 1998. The variable discharge of cortical neurons: implications for connectivity, computation, and information coding. J. Neurosci. 18, 3870–3896.

Whitfield, I.C., Evans, E.F., 1965. Responses of auditory cortical neurons to stimuli of changing frequency. J. Neurophysiol. 28, 655–672.